BJR https://doi.org/10.1259/bjr.20200798

Received: 01 July 2020 | Revised: 06 October 2020 | Accepted: 03 November 2020

Cite this article as:
Van der Cruyssen F, Croonenborghs T-M, Renton T, Hermans R, Politis C, Jacobs R, et al. Magnetic resonance neurography of the head and neck: state of the art, anatomy, pathology and future perspectives. *Br J Radiol* 2021; **94**: 20200798.

REVIEW ARTICLE

Magnetic resonance neurography of the head and neck: state of the art, anatomy, pathology and future perspectives

[1,2]FRÉDERIC VAN DER CRUYSSEN, [1,2]TOMAS-MARIJN CROONENBORGHS, [3]TARA RENTON, [4]ROBERT HERMANS, [1,2]CONSTANTINUS POLITIS, [2,5,6]REINHILDE JACOBS and [7,8,9]JAN CASSELMAN

[1]Department of Oral & Maxillofacial Surgery, University Hospitals Leuven, Leuven, Belgium
[2]Department of Imaging and Pathology, OMFS-IMPATH Research Group, Faculty of Medicine, University Leuven, Leuven, Belgium
[3]Department of Oral Surgery, King's College London Dental Institute, London, UK
[4]Department of Radiology, University Hospitals Leuven, Leuven, Belgium
[5]Department of Oral Health Sciences, KU Leuven and Department of Dentistry, University Hospitals Leuven, Leuven, Belgium
[6]Department of Dental Medicine, Karolinska Institutet, Stockholm, Sweden
[7]Department of Radiology, AZ St-Jan Brugge-Oostende, Bruges, Belgium
[8]Department of Radiology, AZ St-Augustinus, Antwerp, Belgium
[9]Department of Radiology, UZ Gent, Gent, Belgium

Address correspondence to:
Dr Fréderic Van der Cruyssen
E-mail: *frederic.vandercruyssen@uzleuven.be*
Jan Casselman
E-mail: *jan.casselman@azsintjan.be*

ABSTRACT

Magnetic resonance neurography allows for the selective visualization of peripheral nerves and is increasingly being investigated. Whereas in the past, the imaging of the extracranial cranial and occipital nerve branches was inadequate, more and more techniques are now available that do allow nerve imaging. This basic review provides an overview of the literature with current state of the art, anatomical landmarks and future perspectives. Furthermore, we illustrate the possibilities of the three-dimensional CRAnial Nerve Imaging (3D CRANI) MR-sequence by means of a few case studies.

INTRODUCTION

Magnetic resonance neurography (MRN) refers to dedicated MRI sequences that selectively enhance the visualization of peripheral nerves. Several techniques have been described in the literature including two-dimensional (2D) and three-dimensional (3D) T_2 weighted (T_2W) fat suppressed and diffusion-weighted imaging.[1] The first reports on MRN date from 1992 by Howe and Filler and have much evolved since then.[2] At present, MRN is gaining importance due to the introduction of high-field MRI devices and improved imaging techniques.

The skull base course of cranial nerve MRI anatomy has been extensively reviewed.[3–6] In this article, we will review the state of the art and relevant MRN anatomy of the extracranial cranial and occipital nerve branches with illustrative pathologic cases. The author's 3D CRANI MRN sequence will be shared together with its clinical application. This sequence makes useful use of the latest technical developments in MRI research such as compressed sensing and black blood imaging. Assessment methods and benchmark values are cited. Finally, we will discuss some future directions.

State of the art

Although there is well-supported literature on MRN in musculoskeletal imaging, the original research articles are rather limited for the head-neck area. There are several factors why MRN is more difficult to implement in this region. First, the cranial nerves have small calibers and have a complex tortuous course, passing tissues with very different physical properties. The close proximity of fat pads, sinuses and vessels with slow and fast flows require more performant sequences. Ideally, a cranial nerve MRN sequence has a large field of view (FOV) with 3D thin slice thickness, high signal- (SNRs) and contrast-to-noise ratios (CNRs), with uniform fat, venous and arterial suppression and minimal magic angle artifacts. All these requirements

Figure 1. Coronal thick slab (5 mm) MIP/MPR images in the same subject comparing two magnetic resonance neurography techniques. Short arrow: lingual nerve (V_3); long arrow: inferior alveolar nerve (V_3); arrowhead: masseteric nerve (V_3). (a) 3D CRANI sequence. (b) 3D PSIF sequence. 3D, three-dimensional; CRANI, CRAnial Nerve Imaging; MIP, maximum intensity projection; MPR, multiplanar reformatting; PSIF, reversed fast imaging in steady-state free precession.

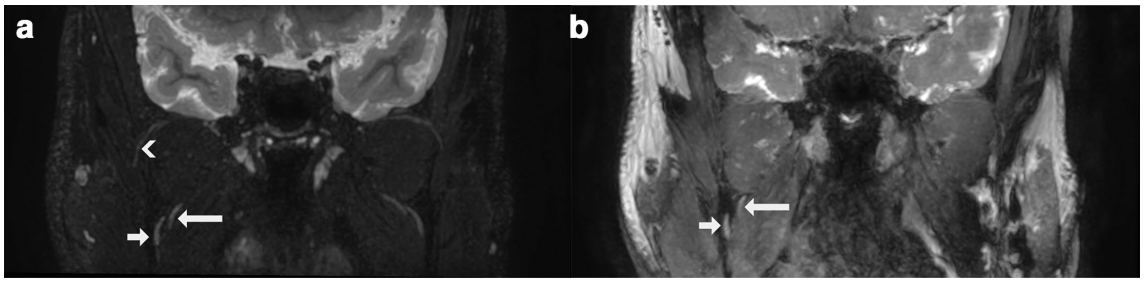

should be met within reasonable acquisition times and minimum chance for motion artifacts. Also, when considering nerve-related pathology we can expect surgical and pathology-induced susceptibility artifacts such as edema, increased vascularity and metal particles, which should be accounted for when possible. Previous reports described cranial nerve anatomy using various MRI sequences such as 3D bFFE (3D balanced fast-field echo sequences), T_2W TSE (turbo spin echo), STIR (short tau inversion recovery) and CISS (constructive interference in steady state).[3–5,7] Although these sequences nicely demonstrate the anatomy, they are not nerve-specific as surrounding structures are not suppressed. In true MRN sequences we try to obtain a heavily T_2W image to achieve high soft tissue contrast with homogenous fat, arterial and venous suppression. Several authors published on available techniques for inferior alveolar, lingual, as well as occipital nerve imaging mainly based on 3D PSIF (reversed fast imaging in steady-state free precession).[8,9] PSIF combines a steady state with a water excitation pulse and fat suppression, selectively enhancing neural anatomy with excellent vascular suppression. A disadvantage of PSIF is the lower SNR and risk for susceptibility artifacts compared to STIR sequences (Figure 1). A protocol suggested by Chhabra et al[9] is further complemented by STIR, CISS, bFFE and DTI (diffusion tensor imaging). By adding multiple sequences, one reduces the risk of non-diagnostic images but loses time and cost-efficiency, which are becoming increasingly important in a health-care environment under financial pressure and with increasing demand for MRI. The authors apply the 3D CRANI (CRAnial Nerve Imaging) sequence which is based on contrast-enhanced black blood 3D STIR TSE preceded by an MSDE (motion-sensitized driven equilibrium) pulse in combination with a pseudo-steady-state sweep and compressed sensing.[10,11] Advantages of 3D CRANI are high SNR and CNR and less susceptibility artifacts. By combining 3D PSIF and 3D CRANI, a cranial MRN examination can be performed in a total acquisition time of 12 min. Table 1 describes in detail the author's MRN protocol including 3D PSIF and 3D CRANI sequences. Routine T1, T_2W and 3D FLAIR (fluid attenuated inversion recovery) brain sequences could be added as well to exclude intracranial pathology. DTI is increasingly being used but, for the time being, mostly remains of scientific value.[10,12,13] In order to obtain a diagnostic MRN acquisition, adequate patient positioning and coil selection is necessary.[6] Thorough patient fixation in mild hyperextension using a 32 channel head coil plays an important role in optimization of the SNR (Figure 2). Others have advocated the use of a 16 channel head neck spine coil.[14] Finally, post-processing using maximum intensity projection (MIP) and multiplanar reformatting (MPR) renders the necessary viewing windows to evaluate the attenuation-enhanced cranial nerves along their trajectory or in non-axial planes according to the radiologist's discretion (Figure 3).[15,16] Routine post-processing software packages allow the necessary reformatting to be carried out such as Philips Volume post-processing package (Philips, Best, Netherlands). Freeware software, *e.g.* Horos (Nimble Co LLC, Annapolis, USA), offers MPR and MIP tools as well.

In the next paragraphs, the cranial and occipital nerve imaging anatomy is described and further illustrated by a Supplementary Video 1.

Trigeminal nerve

Anatomy

The trigeminal nerve has extensive sensory, motor and (para-) sympathetic functions in the orofacial area. The nerve splits into three main divisions before it leaves the skull: ophthalmic nerve (V_1), maxillary nerve (V_2) and mandibular nerve (V_3). The ophthalmic division (V_1) splits into three branches (lacrimal, frontal and nasociliary nerve) which enter the orbit via the superior orbital fissure. The maxillary division (V_2) leaves the cranial cavity via the foramen rotundum and reaches the pterygopalatine fossa. It innervates the teeth of the upper jaw and part of the nasal mucosa. Its dermal branches, the zygomatic nerves and infraorbital nerve, enter via the inferior orbital fissure. The infraorbital nerve runs over the floor of the orbit, it passes through the infraorbital foramen to the skin of the lower eyelid, the side of the nose and part of the upper lip (Figure 4).

The mandibular nerve (V_3) runs through the foramen ovale from the middle cranial fossa to the infratemporal fossa. Three of its four large branches (buccal nerve, inferior alveolar nerve and auriculotemporal nerve) reach the lower skin of the face and are responsible for the cutaneous innervation of the face but it also carries the smaller motor part (radix motoria) which supplies the muscles of mastication. Approximately, 1 cm below the foramen ovale, the trunk of the mandibular nerve splits into an anterior and a posterior division. Its branches are described in three

Table 1. Magnetic resonance neurography sequences for a 3T Philips system (Philips, Best, Netherlands). 3D CRANI and 3D PSIF (reversed fast imaging in steady-state free precession) sequences

	3D CRANI	3D PSIF
Basic MRI technique	3D STIR (TSE)	3D FFE (GE)
TR/TE (ms)	2300/188	12/2.5
FOV (AP/RL/FH mm)	200/200/100	200/164/200
Acquired voxel size (AP/RL/FH mm)	0.9/0.9/0.9 (isotropic)	0.9/0.9/0.9 (isotropic)
Reconstructed voxel size (AP/RL/FH mm)	0.5/0.5/0.45	0.45/0.4/0.4
Slice thickness (mm)	0.5	0.45
Slice oversampling	1.5	1.4
Acquisition time (min:sec)	5:17	6:45
Compressed sensing (acceleration rate)	Yes (3)	No
Flip angle	N/A	35°
Fat suppression technique	STIR	Proset
TSE factor	43 (Startup echoes: 2, linear in Y direction)	N/A
Additional techniques	• MSDE "Black blood" pulse • Pseudo steady state sweep	
Post-processing	MIP/MPR	
Multiplanar reformatting	Orthogonal plane: 5 mm slab thickness with 4.5 mm overlap Curved/oblique planes: 9 mm slap thickness with 8.5 mm overlap	

CRANI, CRAnial Nerve Imaging; FFE, Fast field echo; FOV, Field-of-view; GE, Gradient echo; MIP, Maximum-intensity-projection; MPR, Multiplanar reformatting; MSDE, Motion-sensitized driven equilibrium; N/A, Not applicable; PSIF, reversed fast imaging in steady-state free precession; STIR, Short tau inversion recovery; TE, Echo time; TR, Repetition time; TSE, Turbospin echo.
These can be further supplemented with routine brain T_1W, T_2W, CISS and FLAIR images.

Figure 2. (a) Patient positioning in a standard 32 channel head coil without additional measures. Note the anterior mandible is located outside the coil. (b) Patient positioning after fixation by means of an inflatable pillow with the head in slight hyperextension using a towel roll. The mandible is now well positioned within the coil. (c) Alternative coil, being a 16 channel neck coil. (d) Imaging output after patient positioning as in example (a) Signal loss is seen at the anterior segment. (e) Imaging output after slight hyperextension and thorough fixation as in example (b). (f) Imaging output using a neck coil after patient positioning as in example (c).

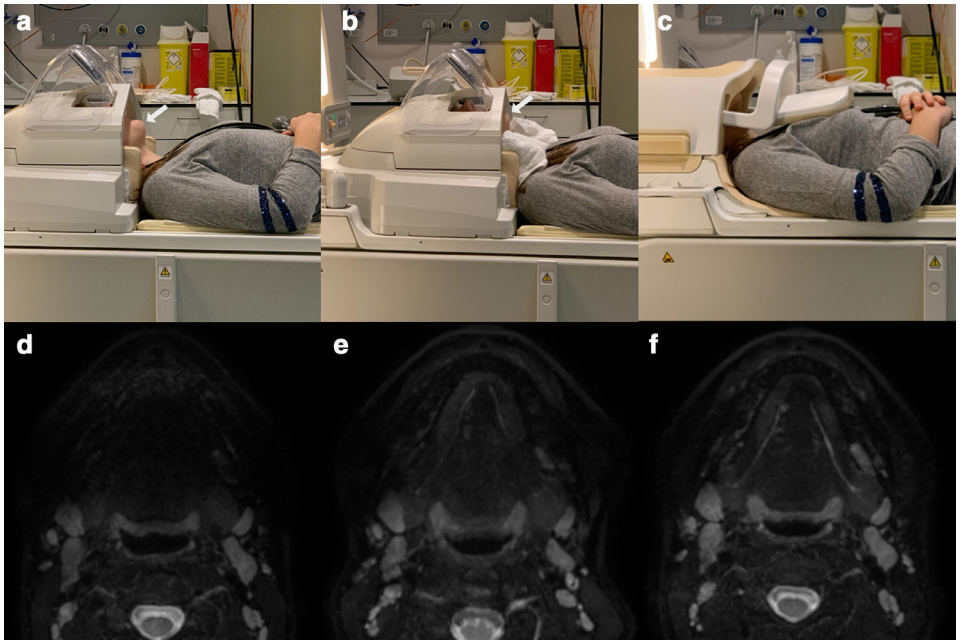

Figure 3. (a) Orthogonal and additional planes constructed in evaluating the cranial and occipital peripheral nerves. Multiplanar reformatting and maximum intensity projection post-processing is applied to visualize the tortuous nerves in the necessary viewing planes. (b) Overall nerve anatomy discussed in this review.

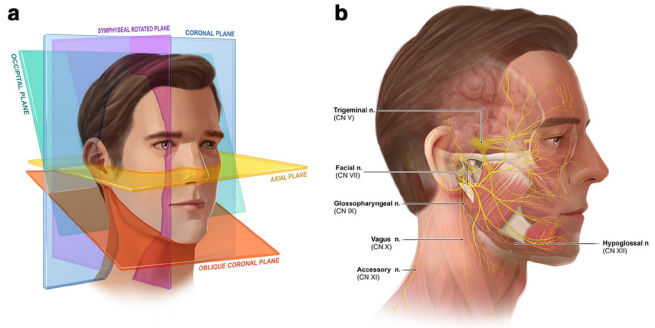

Figure 4. (a) Ophthalmic division of the trigeminal nerve (V_1) using the 3D CRANI sequence. (b) 3D CRANI sequence. Increased caliber of the right infra orbital nerve (V_2) in a patient with Short lasting Unilateral Neuralgiform headache attacks with Conjunctival injection and Tearing (SUNCT) rhinorrhea and forehead sweating. (c) 3D CRANI sequence. Increased signal intensity is noted of the Vidian nerve (V_2) in the same patient as seen in (b). (d) 47-year-old male diagnosed with empty nose syndrome after repeated sinonasal procedures. Marked increase of caliber and signal intensity of both maxillary and infraorbital nerves (arrows) is seen. CRANI, CRAnial Nerve Imaging; SUNCT, short lasting Unilateral Neuralgiform headache attacks with Conjunctival injection and Tearing rhinorrhea and forehead sweating

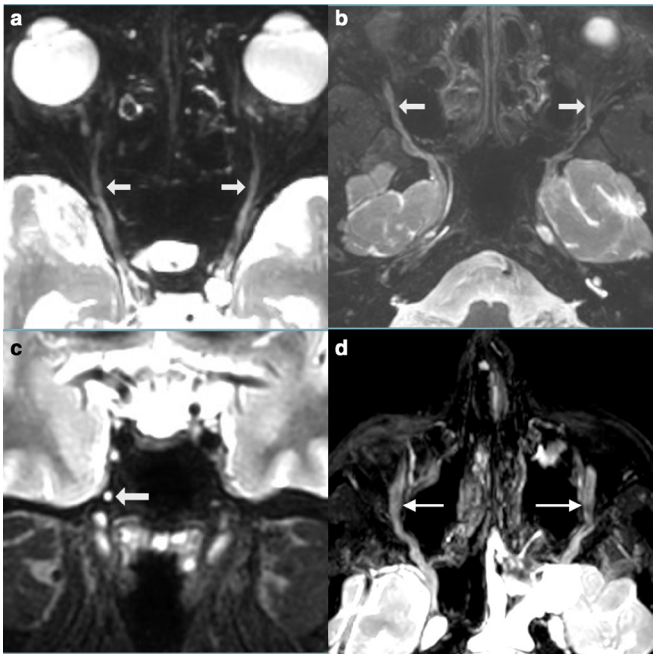

groups (trunk, anterior and posterior division). Branches of the trunk of the mandibular nerve include: the medial pterygoid nerve for the chewing muscle of the same name and meningeal rami.

Branches of the anterior division are all motoric except the buccal nerve which appears between the two heads of lateral pterygoid muscle (Figure 5). The masseteric nerve runs superior from the lateral pterygoid muscle. It passes between the tendon of temporal muscle and the temporomandibular joint (TMJ) and reaches the masseter muscle via the mandibular incisura. On the way, it supplies small branches towards the TMJ. The deep temporal branches, two or three in number, run over the lateral pterygoid muscle to innervate the temporal muscle. The lateral pterygoid nerve innervates the muscle of the same name.

The posterior division of the mandibular nerve constitutes the auriculotemporal, lingual, inferior alveolar and mylohyoid nerve (Figures 5 and 6). The auriculotemporal nerve innervates most of the temporal region and a small part of the auricle (leading edge) and the outer ear canal. The lingual nerve, providing sensory and gustatory innervation to the tongue, appears in the infratemporal fossa between both pterygoid muscles and runs anteroinferiorly over the lateral side of medial pterygoid muscle. The inferior alveolar nerve also ends up between the two pterygoid muscles in the infratemporal fossa. There, it lies behind the lingual nerve. Together with the artery of the same name, it runs between the sphenomandibular ligament towards the inferior alveolar canal or mandibular canal. Just before it enters the mandibular foramen, it releases the mylohyoid nerve that innervates the mylohyoid muscle and anterior belly of the digastric muscle. The inferior alveolar nerve innervates all the teeth of the lower jaw, the adjacent gums and, via its end branch (mental nerve), the skin of the chin and the skin and mucosa of the lower lip.[17–19]

Imaging

The brainstem, cisternal and cavernous trigeminal segments can be imaged using conventional brain sequences including CISS and balanced FFE sequences and have been extensively reviewed in the past.[6,19] The peripheral trigeminal nerve branches are best viewed in multiple planes after thick-slab MIP. The first (V_1), second (V_2) and anterior division of the third division (V_3) can be well depicted on axial views whereas the lingual and inferior alveolar nerve are best seen in a coronal oblique direction (Figures 4–6).

In addition to the neurovascular conflict seen in trigeminal neuralgia cases, more and more neurological abnormalities are becoming detectable. The branches that are mostly involved in pathological conditions are the lingual and inferior alveolar nerve. Their course makes these nerves vulnerable to numerous dental and oromaxillofacial procedures. MRN techniques can aid in grading and clinical decision-making if trauma has occurred.[20] Interested readers are referred to a recent systematic review summarizing the available knowledge base on MRN in post-traumatic trigeminal neuropathies.[21] There is also increasing interest for the use of MRN in orofacial pain patients

Figure 5. (a) Anatomic relation of the anterior division of the mandibular nerve (V_3) best seen in the axial plane. (b) 3D CRANI sequence illustrating the buccal nerve (long arrow), the masseteric nerve (short arrow) and the stem of the auriculotemporal nerve (arrowhead). (c) 3D CRANI sequence in a patient with post-traumatic trigeminal neuropathy of the mandibular division after placement of a titanium temporomandibular joint prosthesis. The left masseteric nerve is thickened and shows an increased signal intensity. CRANI, CRAnial Nerve Imaging

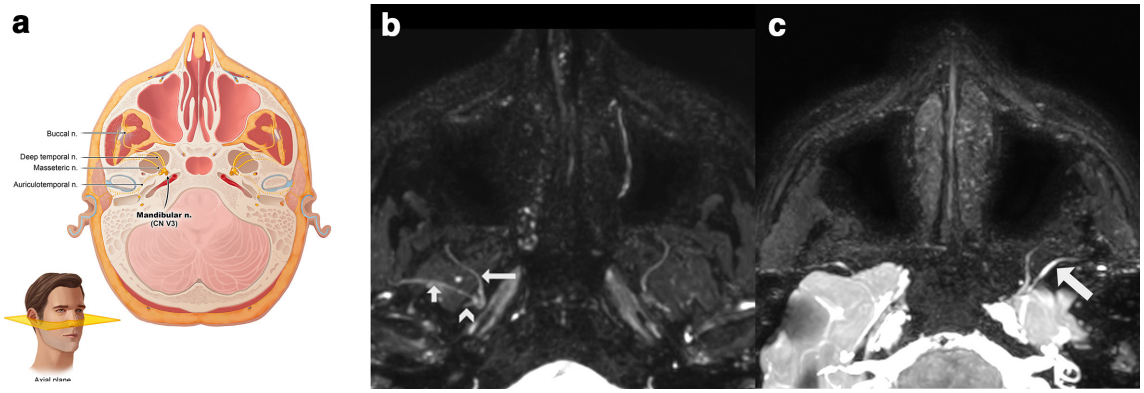

and more specifically in migraine and trigeminal autonomic cephalalgia (Figure 4).[22]

Facial nerve

The facial nerve consists out of motor, sensory and parasympathetic fibers. The sensory fibers innervate a part of the inner ear and the special sensory fibers transport the taste stimuli from the anterior two-thirds of the tongue via the chorda tympani. The parasympathetic fibers innervate the submandibular, sublingual and minor salivary glands, as well as the lacrimal glands. The motor fibers innervate the muscles responsible for the facial expression.

Figure 6. (a) Anatomic overview of the posterior division of the mandibular nerve (V_3) on a coronal oblique plane. (b) Normal appreciation of the lingual (long arrow) and inferior alveolar (short arrow) nerve running between the pterygoid muscles. (c) Right sided post-traumatic trigeminal neuropathy of the inferior alveolar nerve after ramus bone grafting. (d) Patient with neurofibromatosis Type 1, showing bilateral neurofibromas of the inferior alveolar nerve at the level of the mandibular foramen.

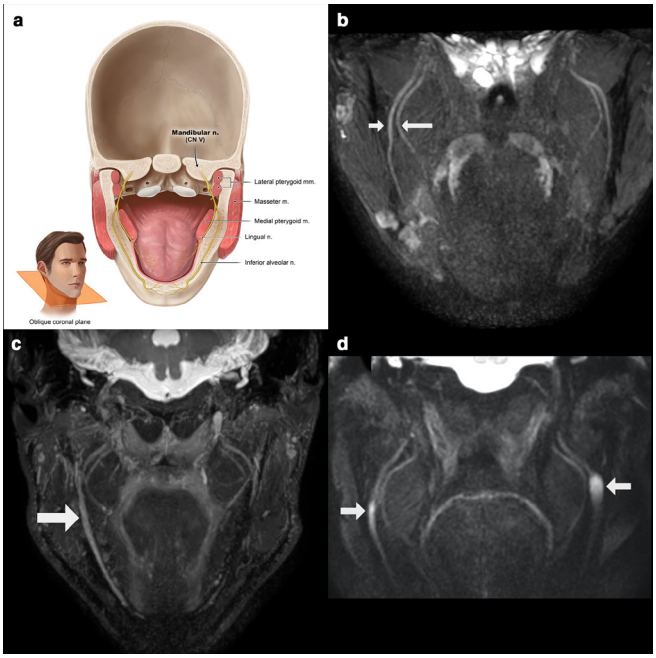

The primary or cisternal segment of the facial nerve leaves the brainstem close to the dorsal pons, transverses the cerebellopontine angle and enters the temporal bone by the porus acousticus in proximity to the vestibulocochlear nerve branches: superior to the cochlear nerve and anterior to the superior and inferior vestibular nerves. The trajectory through the temporal bone is subdivided in a meatal, labyrinthine, tympanic and mastoid segment. The sensory fibers, coming from the intermediate nerve, give on the one hand sensibility to the posterior concha and external auditory canal, on the other hand, the special sensory fibers will form the chorda tympani.

The main trunk of the facial nerve leaves skull base via the stylomastoid foramen, it immediately releases the smaller posterior auricular r. auricularis. Subsequently, the nerve enters the craniomedial part of the parotid gland. Over the intraglandular course the nerve subdivides into five branches, which appear separately at the upper, front and lower edges of this gland. These end branches spread from here to the facial mimic muscles like the spread fingers of a hand resting on the parotid area (temporal, zygomatic, buccal, marginal mandibular and cervical, Figure 6).[23,24]

Imaging

When considering MRI-imaging of the facial nerve, two segments need to be distinguished from each other: the skull base and the extracranial nerve segments. The intracranial and the temporal facial nerve segment is best visualized using 3D CISS, axial T_1W and fat-suppressed T_2W images.[25] Visualization of the facial nerve within the stylomastoid canal, the extracranial and intraparotid part of the VII cranial nerve can be made using

Figure 7. (a) Anatomic overview of the facial nerve and its branches which are best seen on a sagittal slightly rotated or coronal plane. (b) Sagittal view of a normal extracranial facial nerve entering the parotid gland on a 3D CRANI thick-slab MIP/MPR-image. (c) Coronal image with bilateral visualization of the intratemporal and extraforaminal facial nerve after iatrogenic damage on the right side. A slowly recuperative facial nerve paresis occurred after an infiltration with local anesthesia. (d) 60-year-old male with a right sided Bell's palsy. The right extracranial facial (long arrow) nerve shows increased caliber and signal intensity compared to the contralateral facial nerve (short arrow). Discrepancies are noted all the way to the intraparotid course. 3D, three-dimensional; CRANI,CRAnial Nerve Imaging; MIP, maximum intensity projection; MPR, multiplanarreformatting.

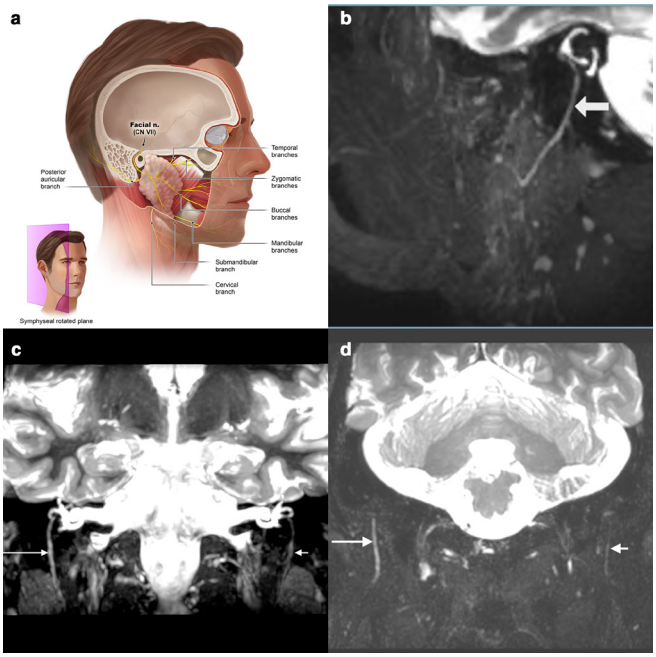

thick-slab MIP/MPR reconstructions of 3D PSIF, and in case of extensive artifacts a black blood 3D-STIR such as 3D CRANI.[9] In case of nerve pathology, an increase of signal intensity and nerve caliber changes can be identified (Figure 7). The use of a 3D PSIF sequence in combination with microsurface coils resulted in superior visualization of the peripheral facial nerve branches, in comparison to a standard head and neck coil, as was reported by Meng et al[26]. The 3D-DESS-WE (double-echo steady state with water excitation) sequence is another established option to be considered for peripheral facial nerve neurography.[27–29]

Cranial nerves IX to XII

The trajectory of the IX, X and XII cranial nerves is anatomically closely intercalated, moreover, a lot of imaging characteristics are similar and therefore they are discussed together (Figure 8).

Glossopharyngeal nerve anatomy

The glossopharyngeal nerve or IX cranial nerve is composed of a combination of motor, sensory and parasympathetic fibers. Firstly, the sensory, gustatory and visceral stimuli are transported via afferent fibers from the retroauricular region, the posterior third of the tongue, the pharynx wall and the tonsils, the soft palate and the eardrum. Secondly, the motor efferents innervate the stylopharyngeus muscle. Thirdly, the parasympathetic fibers stimulate the production of saliva within the parotid gland.[30]

The origin of the IX cranial nerve is strongly associated with the vagus nerve, sharing three functional nuclei in the upper medulla oblongata. The nerve branches from the medulla oblongata within the cerebellomedullary cistern, slightly superior to the vagus nerve. The IX, X and XI cranial nerves course in an anterolateral direction through the cistern to the jugular foramen, exiting the foramen anteriorly from the internal jugular vein. Within the foramen, the glossopharyngeal nerve is known for two focal expansions: a superior node handling general sensible information and a lower node handling visceral sensory, taste and carotid innervations. The extratemporal course of the IX cranial nerve continues in a caudal direction within the carotid space

Figure 8. (a) Anatomic overview of the facial (VII), hypoglossal (XII), glossopharyngeal (IX), vagus (X) and accessory (XI) nerves which can be seen in close relation to each other on a coronal plane. (b) Coronal view after a 3D CRANI sequence indicating the aforementioned peripheral nerves without pathological characteristics. 3D, three-dimensional; CRANI,CRAnial Nerve Imaging.

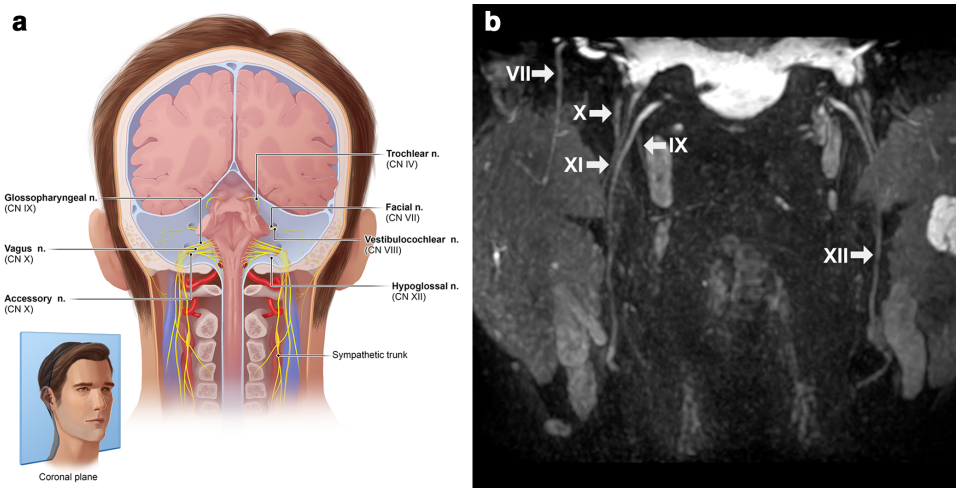

Figure 9. Bilateral normal appreciation of the peripheral hypoglossal nerve (white arrows) on an axial 3D CRANI image after MIP/MPR showing its course around the great vessels before innervating the tongue. 3D, three-dimensional; CRANI, CRAnial Nerve Imaging

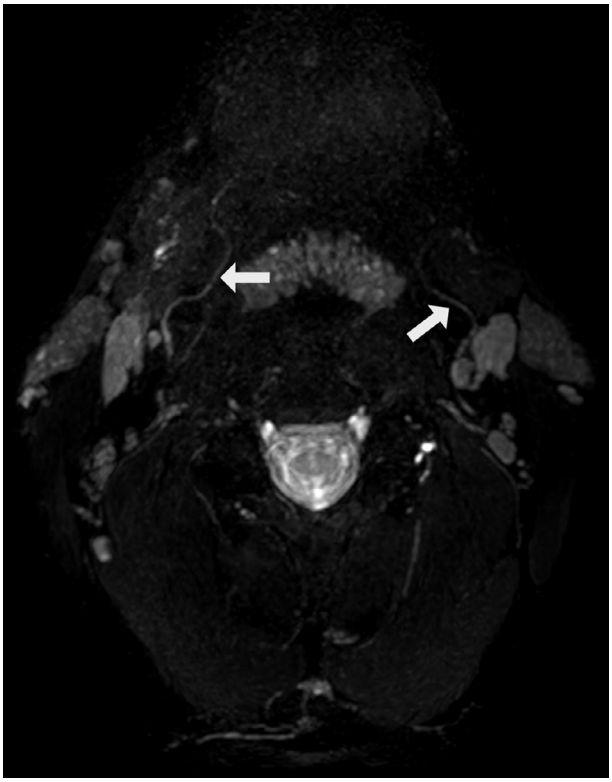

and disperses in five major branches. Firstly, the tympanic nerve branches from the inferior node, carrying sensory information from the external and middle ear and parasympathetic stimuli to the parotid gland via the lesser petrosal nerve. Secondly, the stylopharyngeus branch gives motor input to the stylopharyngeus muscle. Thirdly, the pharyngeal branches associate with branches from the vagus nerve, forming the pharyngeal plexus. Fourthly, the carotid sinus branch mediates parasympathetic information to the carotid body. Finally, the lingual branch conveys general and gustatory sensory input from the posterior third of the tongue.[30,31]

Vagus nerve anatomy

The n. X forms the pharyngeal plexus and mediates the motor function of the soft palate. The parasympathetic fibers of the dorsal motor core of the n. X innervate pharynx, esophagus, trachea, bronchi, lungs, heart, intestines, liver and pancreas.

Multiple rootlets exiting the ventrolateral sulcus, formed by the olive and interior cerebellar peduncle, fuse together in the vagus nerve. The vagus and glossopharyngeal nerve progress closely intercalated through the cerebellopontine angle. Noteworthy, is the small meningeal branch coming from the vagus nerve, innervating the dura within the posterior cranial fossa. Subsequently, the vagus nerve travels through the center of the jugular foramen: superficial to the internal jugular vein and caudal to the glossopharyngeal nerve. Caudally progressing within the carotid space between, however, slightly posterior to the internal carotid artery and internal jugular vein. The internal jugular vein remains lateral and superficial to the vagus nerve; the common carotid artery travels medial and slightly anterior to the nerve.

There are four major extracranial branches leaving the vagus nerve in the head and neck area. Firstly, the auricular branch or Arnold nerve, exiting from the main nerve when passing through the jugular foramen, this nerve receives sensory input coming from the external auditory canal and tympanic membrane. Secondly, the pharyngeal branches leave the vagus nerve below the skull base and form, together with the IX cranial nerve, the pharyngeal plexus innervating the muscles of the soft palate and pharynx. Besides the motor function, the plexus conveys sensory stimuli coming from the epiglottis, trachea and esophagus. Thirdly, the superior laryngeal nerve has a sensory, as well as a motor component. The internal sensory branch conducts sensory input from the hypopharynx, larynx and vocal cords, the external motor branch innervates the cricothyroid and inferior pharyngeal constrictor muscles. And finally, the recurrent laryngeal nerve (RLN) is identified with its renowned asymmetrical anatomical

Figure 10. (a) Anatomic overview of the occipital nerves which are seen together on an oblique axial plane. (b) Lesser (L), third (T) and greater (G) occipital nerves after MIP/MPR on a 3D CRANI sequence in a healthy subject. (c) More distal course of the lesser (L) and greater (G) occipital nerve in a healthy subject. 3D, three-dimensional; CRANI, CRAnial Nerve Imaging; MIP, maximum intensity projection; MPR, multiplanarreformatting.

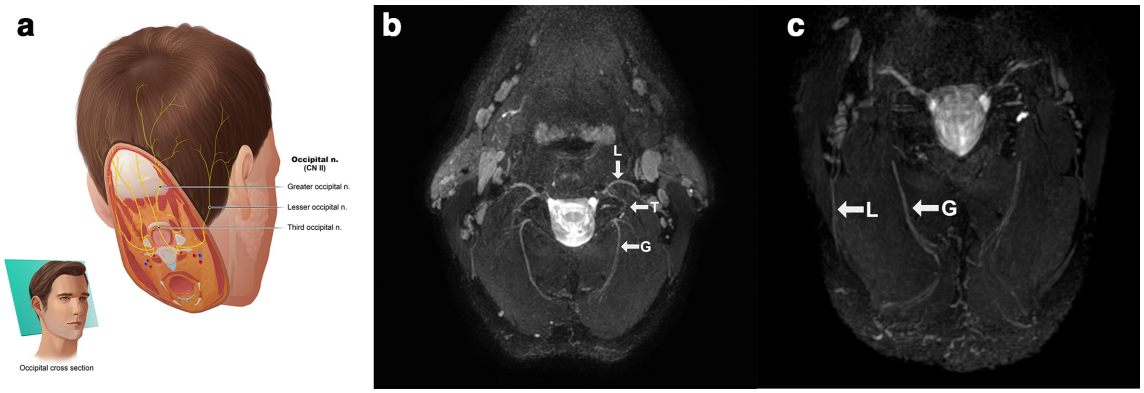

Table 2. Assessment of normal MRN findings and anatomical benchmark nerve diameters (Attention: this does not necessarily correspond to MRN nerve diameters which reflect signal intensities)

Assessment of normal MRN findings			
1. Normal anatomical course 2. Progressive and discrete decrease in caliber and signal intensity towards distal 3. No noticeable sudden interruptions or compressions 4. No perineural scarring 5. No focal swellings and/or signal alterations (no bright-black-bright sign) 6. No abnormalities at the level of the target organs			
Anatomical benchmark nerve diameters			
Nerve	**Site of measurement**	**Mean diameter (mm) ±standard deviation**	**Reference**
Trigeminal nerve			
V1: Ophthalmic division	Middle cranial fossa	1.7 ± 0.1	Pennisiet al[45]
V2: Maxillary division	Middle cranial fossa	4.01 ± 0.52	Zhang et al[46]
V2: infraorbital nerve	Infraorbital foramen	3.30 ± 0.52	Zhang et al[46]
V3: Mandibular division	Middle cranial fossa	7.41 ± 1.41	Soeira et al[47]
V3: Inferior alveolar nerve	Mandibular foramen	2.2 ± 0.4	Ikeda et al[48]
V3: Mental nerve	Mental foramen	1.68–2.37	Gershenson et al[49]
V3: Lingual nerve	Third molar region	3.0 ± 0.5	VonArx et al[50]
V3: Auriculotemporal	After fusion of rootlets	3.18 ± 0.84	Komarnitki et al[51]
Facial nerve			
Segment	Labyrinth	1.13 ± 0.39	Vianna et al[52]
	Tympanic	1.09 ± 0.57	Vianna et al[52]
	Mastoid	1.33 ± 0.65	Vianna et al[52]
	Average between stylomastoid foramen and intraparotid branching	1.4 ± 0.2	Lo et al[53]
Peripheral branch	Intraparotid	0.5 ± 0.1	Tawfik et al[54]
	Temporal branch	0.94 ± 0.33	Martínez Pascual et al[55]
	Zygomatic	1.00 ± 0.46	Martínez Pascual et al[55]
	Buccal	0.99 ± 0.40	Martínez Pascual et al[55]
	Mandibular	0.80 ± 0.34	Martínez Pascual et al[55]
	Cervical	0.83 ± 0.15	Martínez Pascual et al[55]
IX-X-XI nerves			
Glossopharyngeal nerve	Midcervical	Not available	
Vagus nerve	Midcervical	5.1 ± 1.5	Hammer et al[56]
Accessory nerve	Midcervical	Not available	
Hypoglossal nerve			
Segment	Proximal	1.41 ± 1.01	Vacher et al[57]
	Above greater horn of hyoid	1.23 ± 0.77	Vacher et al[57]
	Cervical loop	0.48 ± 0.26	Vacher et al[57]
Occipital nerves			
Greater occipital nerve	After exiting the semispinalis capitis muscle	3.8 ± 1.6	Ducic et al[58]
Lesser occipital nerve	Posterior border of sternocleidomastoid msucle	1.2 ± 1.6	Ducic et al[58]
Third occipital nerve	After exiting the trapezius muscle	1.5 ± 0.3	Tubbs et al[59]

MRN, magnetic resonance neurography.

Figure 11. Panoramic curved reconstruction and MIP of the inferior alveolar nerve using a 3D CRANI sequence allowing a full evaluation at a glance. 3D, three-dimensional; CRANI,CRAnial Nerve Imaging; MIP, maximum intensity projection.

morphology. Bilaterally, the RLN branches from the vagus nerve, it loops around the subclavian artery on the right side and on the left side around the aortic arch. The RLN mediates somatic and visceral sensory input coming from below the vocal cords, moreover, conveying motor output to all laryngeal musculature with exception of the cricothyroid muscle. Hereafter, the vagus nerve continues the trajectory into the thorax.[6,32,33]

Accessory nerve anatomy

The accessory nerve solely contains motor fibers, innervating the sternocleidomastoid as well as the trapezius muscle. The accessory nerve is composed from of both cranial and spinal (C1-5) rootlets. The main trunk of the accessory nerve subsequently travels in a lateral direction, before the nerve leaves the skull via the jugular foramen wherein connections with the vagus nerve can be found. The extracranial accessory nerve runs through the center of the carotid space between the medial internal carotid artery and laterally positioned internal jugular vein (IJV). Subsequently, the nerve divides again in the cranial and spinal roots. The cranial rootlets or internal branches fuse together with the vagus nerve and the spinal rootlets or external branches laterally cross the IJV, passing the transverse process of atlas mostly anteriorly and advancing medially from the styloid process and digastric and stylohyoid muscles. Further progression of the nerve follows an anterolateral direction before reaching the sternocleidomastoid muscle and subsequent formation of a nerve plexus with the ventral rami of C2 to C4, mediating the innervation of the trapezius muscle.[34–36]

Hypoglossal nerve anatomy

The hypoglossal nerve is a purely motor nerve, innervating the extrinsic and intrinsic musculature of the tongue, with exception of the palatoglossus muscle. The XII cranial nerve is formed by two bundles of 10–15 rootlets coming from the ventrolateral sulcus at the medulla oblongata. The bundles pierce through the dura mater separately and fuse together after passing through the hypoglossal canal. The extracranial hypoglossal nerve is joined by efferent C1 motor fibers and progresses laterally and inferiorly to the vagus nerve and internal carotid artery, initially closely associated with the carotid space. Subsequently, after passing the occipital artery, the hypoglossal nerve will turn and mostly pass through the space between carotid arteries and internal jugular vein. After progressing medially to the hyoid tendon of the digastric muscle, the nerve will enter the submandibular space medial to the submandibular gland and hyoglossus muscle (Figure 9). Some of the C1-fibers branch off more cranially and innervate the superior root of the ansa cervicalis, however, other C1 nerve fibers conveying motor input for the geniohyoid and thyrohyoid muscles will remain associated with the XII cranial nerve.[31,37,38]

Glossopharyngeal, vagus, accessory and hypoglossal nerve imaging

Evaluation of the cisternal IX, X and XI cranial nerve segments is preferably performed using heavily T_2W steady-state free precession imaging sequences.[25] However, these 2D sequences have mainly been replaced by 3D CISS and 3D FIESTA.[3] The distinct foraminal nerve segments are identified using conventional 3D FIESTA, or CE-MRA (contrast-enhanced magnetic resonance angiograph) as described by Linn et al[39].[5] The below-skull-base-related nerve segments can be nicely differentiated on the MIP/MPR-reformatted 3D CRANI images (Figures 8 and 9). They are conveniently identified on coronal and axial planes. As discussed by Chhabra and colleagues, 3D PSIF is also a valuable technique for neurography of these closely intercalated cranial nerves.[20] The typical nerve trajectories can be distinguished as follows, the extracranial vagus nerve is positioned between the medial IX and lateral XII nerve and has the largest diameter.

Figure 12. 3D fusion of CT and MRN images which can be valuable in planning the placement of a custom made temporomandibular joint prosthesis (blue outline). The inferior alveolar nerve is segmented (red outline) and indicated (white arrows) before entering the mandibular canal. 3D, three-dimensional; MRN, magnetic resonance neurography.

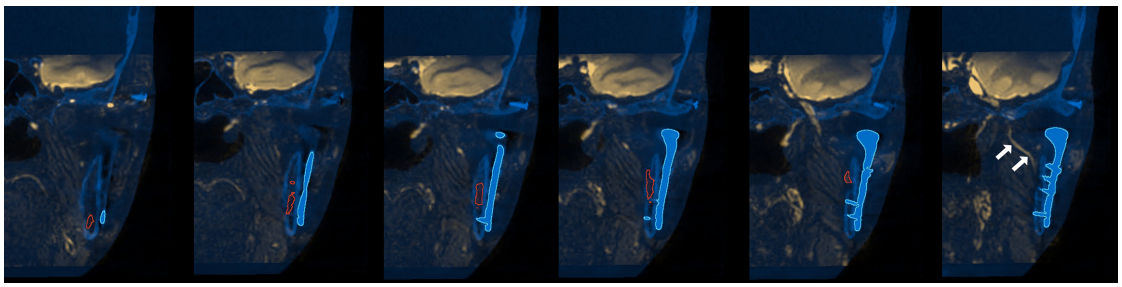

Table 3. Possible MRN indications in the head and neck area

Indication	Reference
Chronic demyelinating neuropathies	Own experience, unpublished
Cranial neuralgias	Hwang et al[22]
Follow-up of regeneration (*e.g.* after nerve surgery)	Not available
Traumatic neuropathies • Maxillofacial trauma • Post-traumatic cranial neuropathies	Burian et al[73], Dessouky et al[20], Zuniga et al[62]
Nerve sheath tumors	Chhabra et al[74]
Surgical planning involving cranial nerves	Dessouky et al[20]
Viral, bacterial neuritis (*e.g.* Bell's palsy)	Own experience, unpublished

MRN, magnetic resonance neurography.

Occipital nerves (C2)

Anatomy

The greater occipital nerve (GON) ensues from the fusion of nerve fibers coming from the medial branch of the dorsal ramus of the second and, to a lesser degree, the third spinal nerve. At the level of the C1-C2 vertebrae, the nerve travels in the occipital direction between the medial inferior capitis oblique and lateral semispinal muscles. Important anatomical variation is described concerning the penetration of the trapezius, semispinalis capitis and inferior capitis oblique muscles which are pierced by GON in respectively, 45, 7,5 and 90% of cases.[40] Next, the nerve loops upwards, joins the occipital artery and subdivides in a medial and lateral branch before terminal branches ensue.[40–43]

The lesser occipital nerve (LON) typically originates from the ventral rami of spinal nerves C2 and C3. The nerve loops around the sternocleidomastoid muscle (SCM). Its trajectory is parallel to the posterior border of the SCM, piercing the superficial lamina of the cervical fascia, in direction of the occipital area. Finally, the LON divides into medial and lateral branches in the middle between the intermastoid line and inion. Interconnections or overlap of GON and LON branches are frequently present.[42–44]

The third occipital nerve (TON) derives from the superficial medial branch of the dorsal ramus of the third spinal nerve. The nerve courses on top of the dorsolateral surface of the C2-C3 facet joint. The TON travels deeply to the semispinalis capitis muscle in a posterior direction when a communicating branch to GON exits. The overlying musculature will be pierced by TON before progressing subcutaneously.[33,40,42,43]

Functionally, GON, LON and TON receive somatic sensory input from the occipital region. The semispinalis muscle will receive motor output via GON, and to a lesser degree from TON (Figure 10).[33,42,43]

Imaging

The occipital nerves are easily visualized on a slightly oblique axial plane using 3D PSIF or 3D CRANI sequences and are of increasing interest to neurologists and pain specialists. Pathological thickening and signal alterations can be noted in cases of occipital neuralgia also referred to as occipital migraine.[22] Occasionally, one can also detect pathological changes after trauma or surgery in this region (Figure 10).

MRN assessment

The evaluation of the extraforaminal cranial nerves and possible abnormalities is best performed systematically. A proposal is presented in Table 2. At present, large series with benchmark values for each nerve segment are lacking in order to distinguish pathology from normal. Studies are underway to report these normal values.[60–62] However, internal validation is always possible with the contralateral side. When bilateral abnormalities occur, a possible problem arises, but in combination with the clinical picture and focal changes, there is usually no diagnostic problem. Table 2 includes anatomical benchmark values for the discussed cranial and occipital nerves. We should remain cautious with external validation of nerve thickness and signal intensity as MR sequences are not actual anatomical representations but representations of signal intensity. Therefore, caution should be exercised when comparing MR parameters with published reference values. For the time being, internal comparison with the non-pathological side is the most reliable method. Interested readers are referred to the excellent review papers by Chhabra et al[5,9,63].

Future perspectives

MRN performance and applications are evolving rapidly. Where 0.5 T systems were available 20 years ago, we are now seeing the arrival of clinical 7 T and higher. The introduction of these high-field MRI devices can further improve spatial resolution and soft tissue contrast. However, there is also a risk of increasing susceptibility artifacts as they increase with increasing field strength and thus, they should not be considered the holy grail in MRN imaging. Rather a combination of high-field systems, specialized coils, improved post-processing and contrast agents will likely evolve this field in the next phase.[26,64,65] First, there is a need to further define anatomical benchmarks for the cranial nerves. Several authors have described reference values for the trigeminal nerve or provided classifications to define degree of nerve injury.[14,62] Next, there is a whole field of research left to obtain functional information by means of DTI and diffusion tensor tractography (DTT). These techniques are based on differences in diffusion of protons along nerve tracts and allow quantification of diffusion restriction by means of the apparent diffusion coefficient (ADC) and fractional anisotropy (FA) values. In combination with morphological changes, a more detailed description of neural dysfunction and neuroregeneration becomes reality.[66] Additionally, they allow for a multiparametric and standardized approach towards nerve injuries and pathology, which is currently lacking. Several studies described the successful application of DTI and DTT in extraforaminal cranial nerve imaging.[12,67–70] But, most reports only describe DTT of the proximal nerve branches with varying reference values.[68,71] DTT of the small distal cranial nerve branches

remains challenging and, for the time being, is mostly of scientific value.[13,72] In addition to strong diagnostic value, MRN also offers applications for planning of surgical procedures. Current indications are summarized in Table 3. The surgeon could check in advance where the nerve is located in relation to the neoplasia or when the anatomy deviates from the normal.[68] Panoramic reconstructions can aid in dental surgery planning (Figure 11).[75] Fusion with CT images could help with the placement of a TMJ prosthesis near these peripheral nerve branches (Figure 12) and it is only a matter of time before artificial intelligence aids find their way to the clinic.[76,77] The current paper is based on only a handful studies published by a limited number of centers. Large studies on MRN applications in the head and neck area are lacking. Most studies are still in a feasibility phase. There is a need for more high-quality research to further validate these techniques for the various applications in the coming years. In conclusion, the field of MRN is still in its infancy but a wide range of applications are already under development. It is therefore important that radiologists and anyone involved in cranial nerve pathology become familiar with these techniques and their possibilities.

REFERENCES

1. Chhabra A, Andreisek G, Soldatos T, Wang KC, Flammang AJ, Belzberg AJ, et al. Mr neurography: past, present, and future. *AJR Am J Roentgenol* 2011; **197**: 583–91. doi: https://doi.org/10.2214/AJR.10.6012
2. Howe FA, Filler AG, Bell BA, Griffiths JR. Magnetic resonance neurography. *Magn Reson Med* 1992; **28**: 328–38. doi: https://doi.org/10.1002/mrm.1910280215
3. Blitz AM, Macedo LL, Chonka ZD, Ilica AT, Choudhri AF, Gallia GL, et al. High-Resolution CISS MR imaging with and without contrast for evaluation of the upper cranial nerves: segmental anatomy and selected pathologic conditions of the cisternal through extraforaminal segments. *Neuroimaging Clin N Am* 2014; **24**: 17–34. doi: https://doi.org/10.1016/j.nic.2013.03.021
4. Hiwatashi A, Yoshiura T, Yamashita K, Kamano H, Honda H. High-resolution stir for 3-T MRI of the posterior fossa: visualization of the lower cranial nerves and arteriovenous structures related to neurovascular compression. *AJR Am J Roentgenol* 2012; **199**: 644–8. doi: https://doi.org/10.2214/AJR.11.6566
5. Blitz AM, Choudhri AF, Chonka ZD, Ilica AT, Macedo LL, Chhabra A, et al. Anatomic considerations, nomenclature, and advanced cross-sectional imaging techniques for visualization of the cranial nerve segments by MR imaging. *Neuroimaging Clin N Am* 2014; **24**: 1–15. doi: https://doi.org/10.1016/j.nic.2013.03.020
6. Casselman J, Mermuys K, Delanote J, Ghekiere J, Coenegrachts K. MRI of the cranial nerves—more than meets the eye: technical considerations and advanced anatomy. *Neuroimaging Clin N Am* 2008; **18**: 197–231. doi: https://doi.org/10.1016/j.nic.2008.02.002
7. Lee JH, Cheng K-L, Choi YJ, Baek JH. High-Resolution imaging of neural anatomy and pathology of the neck. *Korean J Radiol* 2017; **18**: 180Available from. doi: https://doi.org/10.3348/kjr.2017.18.1.180
8. Zhang Z, Meng Q, Chen Y, Li Z, Luo B, Yang Z, et al. 3-T imaging of the cranial nerves using three-dimensional reversed FISP with diffusion-weighted Mr sequence. *J Magn Reson Imaging* 2008; **27**: 454–8. doi: https://doi.org/10.1002/jmri.21009
9. Chhabra A, Bajaj G, Wadhwa V, Quadri RS, White J, Myers LL, et al. Mr Neurographic evaluation of facial and neck pain: normal and abnormal craniospinal nerves below the skull base. *RadioGraphics* 2018; **38**: 1498–513. doi: https://doi.org/10.1148/rg.2018170194
10. Klupp E, Cervantes B, Sollmann N, Treibel F, Weidlich D, Baum T, et al. Improved brachial plexus visualization using an adiabatic iMSDE-Prepared stir 3D TSE. *Clin Neuroradiol* 2019; **29**: 631–8. doi: https://doi.org/10.1007/s00062-018-0706-0
11. Yoneyama M, Takahara T, Kwee TC, Nakamura M, Tabuchi T. Rapid high resolution Mr neurography with a diffusion-weighted pre-pulse. *Magn Reson Med Sci* 2013; **12**: 111–9. doi: https://doi.org/10.2463/mrms.2012-0063
12. Saito S, Ozawa H, Fujioka M, Hikishima K, Hata J, Kurihara S, et al. Visualization of nerve fibers around the carotid bifurcation with use of a 9.4 tesla microscopic magnetic resonance diffusion tensor imaging with tractography. *Head Neck* 2018; **40**: 2228–34. doi: https://doi.org/10.1002/hed.25318
13. Jacquesson T, Frindel C, Kocevar G, Berhouma M, Jouanneau E, Attyé A, et al. Overcoming challenges of cranial nerve tractography: a targeted review. *Neurosurgery* 2019; **84**: 313–25. doi: https://doi.org/10.1093/neuros/nyy229
14. Burian E, Probst FA, Weidlich D, Cornelius C-P, Maier L, Robl T, et al. MRI of the inferior alveolar nerve and lingual nerve-anatomical variation and morphometric benchmark values of nerve diameters in healthy subjects. *Clin Oral Investig* 2020; **24**: 2625–34. doi: https://doi.org/10.1007/s00784-019-03120-7
15. Dalrymple NC, Prasad SR, Freckleton MW, Chintapalli KN. Informatics in radiology (infoRAD): introduction to the language of three-dimensional imaging with multidetector CT. *Radiographics* 2005; **25**: 1409–28. doi: https://doi.org/10.1148/rg.255055044
16. Napel S, Rubin GD, Jeffrey RB. STS-MIP: a new reconstruction technique for CT of the chest. *J Comput Assist Tomogr* 1993; **17**: 832–8.
17. Joo W, Yoshioka F, Funaki T, Mizokami K, Rhoton AL. Microsurgical anatomy of the trigeminal nerve. *Clin. Anat.* 2014; **27**: 61–88. doi: https://doi.org/10.1002/ca.22330
18. Woolfall P, Coulthard A. Pictorial review: trigeminal nerve: anatomy and pathology. *Br J Radiol* 2001; **74**: 458–67. doi: https://doi.org/10.1259/bjr.74.881.740458
19. Bathla G, Hegde AN. The trigeminal nerve: an illustrated review of its imaging anatomy and pathology. *Clin Radiol* 2013; **68**: 203–13. doi: https://doi.org/10.1016/j.crad.2012.05.019
20. Dessouky R, Xi Y, Zuniga J, Chhabra A. Role of Mr neurography for the diagnosis of peripheral trigeminal nerve injuries in patients with prior molar tooth extraction. *AJNR Am J Neuroradiol* 2018; **39**: 162–9. doi: https://doi.org/10.3174/ajnr.A5438
21.21. Van der Cruyssen F, Peeters F, Croonenborghs T-M, Fransen J, Renton T, Politis C, et al. A systematic review on diagnostic test accuracy of magnetic resonance neurography versus clinical neurosensory assessment for post-traumatic trigeminal neuropathy in patients reporting neurosensory disturbance. *Dentomaxillofac Radiol* 2020;: 20200103. doi: https://doi.org/10.1259/dmfr.20200103

22. Hwang L, Dessouky R, Xi Y, Amirlak B, Chhabra A. Mr neurography of greater occipital nerve neuropathy: initial experience in patients with migraine. *AJNR Am J Neuroradiol* 2017; **38**: 2203–9. doi: https://doi.org/10.3174/ajnr.A5354
23. Gupta S, Mends F, Hagiwara M, Fatterpekar G, Roehm PC. Imaging the facial nerve: a contemporary review. *Radiol Res Pract* 2013; **2013**: 1–14. doi: https://doi.org/10.1155/2013/248039
24. Myckatyn TM, Mackinnon SE. A review of facial nerve anatomy. *Semin Plast Surg* 2004; **18**: 5–11. doi: https://doi.org/10.1055/s-2004-823118
25. Casselman JW, Kuhweide R, Deimling M, Ampe W, Dehaene I, Meeus L. Constructive interference in steady state-3DFT MR imaging of the inner ear and cerebellopontine angle. *AJNR Am J Neuroradiol* 1993; **14**: 47–57.
26. Meng Q, Guan J, Rao L, Chu J, Li S, Zhou Z, et al. High-Resolution MRI of the intraparotid facial nerve based on a Microsurface coil and a 3D reversed fast imaging with steady-state precession DWI sequence at 3T. *Am J Neuroradiol* 2013; **34**: 1643–8.
27. Wen J, Desai NS, Jeffery D, Aygun N, Blitz A. High-Resolution isotropic three-dimensional MR imaging of the Extraforaminal segments of the cranial nerves. *Magn Reson Imaging Clin N Am* 2018; **26**: 101–19Available from. doi: https://doi.org/10.1016/j.mric.2017.08.007
28. Fujii H, Fujita A, Yang A, Kanazawa H, Buch K, Sakai O, et al. Visualization of the peripheral branches of the mandibular division of the trigeminal nerve on 3D Double-Echo steady-state with water excitation sequence. *AJNR Am J Neuroradiol* 2015; **36**: 1333–7. doi: https://doi.org/10.3174/ajnr.A4288
29. Fujii H, Fujita A, Kanazawa H, Sung E, Sakai O, Sugimoto H. Localization of parotid gland tumors in relation to the intraparotid facial nerve on 3D Double-Echo steady-state with water excitation sequence. *AJNR Am J Neuroradiol* 2019; **40**: 1037–42. doi: https://doi.org/10.3174/ajnr.A6078
30. García Santos JM, Sánchez Jiménez S, Tovar Pérez M, Moreno Cascales M, Lailhacar Marty J, Fernández-Villacañas Marín MA. Tracking the glossopharyngeal nerve pathway through anatomical references in cross-sectional imaging techniques: a pictorial review. *Insights Imaging* 2018; **9**: 559–69. doi: https://doi.org/10.1007/s13244-018-0630-5
31. Sakamoto Y. Morphological features of the branching pattern of the hypoglossal nerve. *Anat Rec* 2019; **302**: 558–67. doi: https://doi.org/10.1002/ar.23819
32. Yuan H, Silberstein SD. Vagus nerve and vagus nerve stimulation, a comprehensive review: Part I. *Headache* 2016; **56**: 71–8. doi: https://doi.org/10.1111/head.12647
33. Tubbs RS, Mortazavi MM, Loukas M, D'Antoni AV, Shoja MM, Chern JJ, et al. Anatomical study of the third occipital nerve and its potential role in occipital headache/neck pain following midline dissections of the craniocervical junction. *J Neurosurg* 2011; **15**: 71–5. doi: https://doi.org/10.3171/2011.3.SPINE10854
34. Durazzo MD, Furlan JC, Teixeira GV, Friguglietti CUM, Kulcsar MAV, Magalhães RP, et al. Anatomic landmarks for localization of the spinal accessory nerve. *Clin. Anat.* 2009; **22**: 471–5. doi: https://doi.org/10.1002/ca.20796
35. Johal J, Iwanaga J, Tubbs K, Loukas M, Oskouian RJ, Tubbs RS. The accessory nerve: a comprehensive review of its anatomy, development, variations, landmarks and clinical considerations. *Anat Rec* 2019; **302**: 620–9. doi: https://doi.org/10.1002/ar.23823
36. Overland J, Hodge JC, Breik O, Krishnan S. Surgical anatomy of the spinal accessory nerve: review of the literature and case report of a rare anatomical variant. *J. Laryngol. Otol.* 2016; **130**: 969–72. doi: https://doi.org/10.1017/S0022215116008148
37. Kim DD, Caccamese JF, Ord RA. Variations in the course of the hypoglossal nerve: a case report and literature review. *Int J Oral Maxillofac Surg* 2003; **32**: 568–70. doi: https://doi.org/10.1016/S0901-5027(02)90360-2
38. Lin H, Barkhaus P. Cranial nerve XII: the hypoglossal nerve. *Semin Neurol* 2009; **29**: 045–52. doi: https://doi.org/10.1055/s-0028-1124022
39. Linn J, Peters F, Moriggl B, Naidich TP, Brückmann H, Yousry I. The jugular foramen: imaging strategy and detailed anatomy at 3T. *AJNR Am J Neuroradiol* 2009; **30**: 34–41. doi: https://doi.org/10.3174/ajnr.A1281
40. Bovim G, Bonamico L, Fredriksen TA, Lindboe CF, Stolt-Nielsen A, Sjaastad O. Topographic variations in the peripheral course of the greater occipital nerve. *Spine* 1991; **16**: 475–8. doi: https://doi.org/10.1097/00007632-199104000-00017
41. Mosser SW, Guyuron B, Janis JE, Rohrich RJ. The anatomy of the greater occipital nerve: implications for the etiology of migraine headaches. *Plast Reconstr Surg* 2004; **113**: 693–7. doi: https://doi.org/10.1097/01.PRS.0000101502.22727.5D
42. Kwon H-J, Kim H-S, O J, Kang HJ, Won JY, Yang H-M, et al. Anatomical analysis of the distribution patterns of occipital cutaneous nerves and the clinical implications for pain management. *J Pain Res* 2018; **11**: 2023–31. doi: https://doi.org/10.2147/JPR.S175506
43. Cohen-Gadol A, Kemp III W, Tubbs RShane, Rs T. The innervation of the scalp: a comprehensive review including anatomy, pathology, and neurosurgical correlates. *Surg Neurol Int* 2011; **2**: 178. doi: https://doi.org/10.4103/2152-7806.90699
44. Lee M, Brown M, Chepla K, Okada H, Gatherwright J, Totonchi A, et al. An anatomical study of the lesser occipital nerve and its potential compression points: implications for surgical treatment of migraine headaches. *Plast Reconstr Surg* 2013; **132**: 1551–6. doi: https://doi.org/10.1097/PRS.0b013e3182a80721
45. Pennisi E, Cruccu G, Manfredi M, Palladini G. Histometric study of myelinated fibers in the human trigeminal nerve. *J Neurol Sci* 1991; **105**: 22–8. doi: https://doi.org/10.1016/0022-510X(91)90113-L
46. Zhang Y-xin, Zhang K-qi, Qin S-jia, Wang F. Autopsy study for maxillary nerve and its artery supply. *Zhonghua Er Bi Yan Hou Tou Jing Wai Ke Za Zhi* 2012; **47**: 836–40.
47. Soeira G, Abd el-Bary TH, Dujovny M, Slavin KV, Ausman JI. Microsurgical anatomy of the trigeminal nerve. *Neurol Res* 1994; **16**: 273–83. doi: https://doi.org/10.1080/01616412.1994.11740240
48. Ikeda K, Ho KC, Nowicki BH, Haughton VM. Multiplanar Mr and anatomic study of the mandibular canal. *AJNR Am J Neuroradiol* 1996; **17**: 579–84.
49. Gershenson A, Nathan H, Luchansky E. Mental foramen and mental nerve: changes with age. *Cells Tissues Organs* 1986; **126**: 21–8. doi: https://doi.org/10.1159/000146181
50. von Arx T, Lozanoff S. *Clinical oral anatomy*. Switzerland: Springer International Publishing; 2017. pp. 561.
51. Komarnitki I, Andrzejczak-Sobocińska A, Tomczyk J, Deszczyńska K, Ciszek B. Clinical anatomy of the auriculotemporal nerve in the area of the infratemporal fossa. *Folia Morphol* 2012; **71**: 187–93.
52. Vianna M, Adams M, Schachern P, Lazarini PR, Paparella MM, Cureoglu S. Bell's palsy — A 3-dimensional temporal bone study. *Otol Neurotol* 2014; **35**: 514–8.
53. YL L, Fook-Chong S, Leoh TH, Dan YF, Lee MP, Gan HY, et al. High-resolution ultrasound in the evaluation and prognosis of Bell's palsy. *Eur J Neurol* 2010; **17**: 885–9.
54. Tawfik EA. Sonographic characteristics of the facial nerve in healthy volunteers. *Muscle*

Nerve 2015; **52**: 767–71. doi: https://doi.org/10.1002/mus.24627
55. Martínez Pascual P, Maranillo E, Vázquez T, Simon de Blas C, Lasso JM, Sañudo JR. Extracranial course of the facial nerve revisited. *Anat Rec* 2019; **302**: 599–608. doi: https://doi.org/10.1002/ar.23825
56. Hammer N, Löffler S, Cakmak YO, Ondruschka B, Planitzer U, Schultz M, et al. Cervical vagus nerve morphometry and vascularity in the context of nerve stimulation - A cadaveric study. *Sci Rep* 2018; **8**: 1–9. doi: https://doi.org/10.1038/s41598-018-26135-8
57. Vacher C, Dauge M-C. Morphometric study of the cervical course of the hypoglossal nerve and its application to hypoglossal facial anastomosis. *Surg Radiol Anat* 2004; **26**: 86–90. doi: https://doi.org/10.1007/s00276-003-0197-8
58. Ducic I, Moriarty M, Al-Attar A. Anatomical variations of the occipital nerves: implications for the treatment of chronic headaches. *Plast Reconstr Surg* 2009; **123**: 859–63. doi: https://doi.org/10.1097/PRS.0b013e318199f080
59. Tubbs RS, Mortazavi MM, Loukas M, D'Antoni AV, Shoja MM, Chern JJ, et al. Anatomical study of the third occipital nerve and its potential role in occipital headache/neck pain following midline dissections of the craniocervical junction. *J Neurosurg* 2011; **15**: 71–5. doi: https://doi.org/10.3171/2011.3.SPINE10854
60. Burian E, Probst FA, Weidlich D, Cornelius C-P, Maier L, Robl T, et al. Mri of the inferior alveolar nerve and lingual nerve-anatomical variation and morphometric benchmark values of nerve diameters in healthy subjects. *Clin Oral Investig* 2020; **24**: 2625–34. doi: https://doi.org/10.1007/s00784-019-03120-7
61. Cox B, Zuniga JR, Panchal N, Cheng J, Chhabra A. Magnetic resonance neurography in the management of peripheral trigeminal neuropathy: experience in a tertiary care centre. *Eur Radiol* 2016; **26**: 3392–400. doi: https://doi.org/10.1007/s00330-015-4182-5
62. Zuniga JR, Mistry C, Tikhonov I, Dessouky R, Chhabra A. Magnetic resonance neurography of traumatic and nontraumatic peripheral trigeminal neuropathies. *J Oral Maxillofac Surg* 2018; **76**: 725–36. doi: https://doi.org/10.1016/j.joms.2017.11.007
63. Chhabra A JAP, Ph D, Flammang A, Gilson W, Carrino JA. Magnetic resonance neurography – techniques and interpretation. *Magnetom flash-Clinical Neurol* 2012; **2**: 4–8.
64. Voskuilen L, de Heer P, van der Molen L, Balm AJM, van der Heijden F, Strijkers GJ, et al. A 12-channel flexible receiver coil for accelerated tongue imaging. *MAGMA* 2020; **33**: 581–90. doi: https://doi.org/10.1007/s10334-019-00824-5
65. Wessig C, Bendszus M, Stoll G. In vivo visualization of focal demyelination in peripheral nerves by gadofluorine M-enhanced magnetic resonance imaging. *Exp Neurol* 2007; **204**: 14–19. doi: https://doi.org/10.1016/j.expneurol.2006.09.022
66. Takagi T, Nakamura M, Yamada M, Hikishima K, Momoshima S, Fujiyoshi K, et al. Visualization of peripheral nerve degeneration and regeneration: monitoring with diffusion tensor tractography. *Neuroimage* 2009; **44**: 884–92. doi: https://doi.org/10.1016/j.neuroimage.2008.09.022
67. El Kininy W, Roddy D, Davy S, Roman E, O'Keane V, O'Hanlon E, El KW, O'Keefe V, O'Hanlon E, et al. Magnetic resonance diffusion weighted imaging using constrained spherical deconvolution-based tractography of the extracranial course of the facial nerve. *Oral Surg Oral Med Oral Pathol Oral Radiol* 2020; **130**: 1–13. doi: https://doi.org/10.1016/j.oooo.2019.12.012
68. Rouchy R-C, Attyé A, Medici M, Renard F, Kastler A, Grand S, et al. Facial nerve tractography: a new tool for the detection of perineural spread in parotid cancers. *Eur Radiol* 2018; **28**: 3861–71. doi: https://doi.org/10.1007/s00330-018-5318-1
69. Xie G, Zhang F, Leung L, Mooney MA, Epprecht L, Norton I, et al. Anatomical assessment of trigeminal nerve tractography using diffusion MRI: a comparison of acquisition b-values and single- and multi-fiber tracking strategies. *Neuroimage Clin* 2020; **25**: 102160. doi: https://doi.org/10.1016/j.nicl.2019.102160
70. Terumitsu M, Matsuzawa H, Seo K, Watanabe M, Kurata S, Suda A, et al. High-Contrast high-resolution imaging of posttraumatic mandibular nerve by 3DAC-PROPELLER magnetic resonance imaging: correlation with the severity of sensory disturbance. *Oral Surg Oral Med Oral Pathol Oral Radiol* 2017; **124**: 85–94. doi: https://doi.org/10.1016/j.oooo.2017.02.017
71. Shapey J, Vos SB, Vercauteren T, Bradford R, Saeed SR, Bisdas S, et al. Clinical applications for diffusion MRI and tractography of cranial nerves within the posterior fossa: a systematic review. *Front Neurosci* 2019; **13**: 23. doi: https://doi.org/10.3389/fnins.2019.00023
72. Cauley KA, Filippi CG. Diffusion-tensor imaging of small nerve bundles: cranial nerves, peripheral nerves, distal spinal cord, and lumbar nerve roots-clinical applications. *AJR Am J Roentgenol* 2013; **201**: W326–35. doi: https://doi.org/10.2214/AJR.12.9230
73. Burian E, Sollmann N, Ritschl LM, Palla B, Maier L, Zimmer C, et al. High resolution MRI for quantitative assessment of inferior alveolar nerve impairment in course of mandible fractures: an imaging feasibility study. *Sci Rep* 2020; **10**: 1–9. doi: https://doi.org/10.1038/s41598-020-68501-5
74. Chhabra A, Madhuranthakam AJ, Andreisek G. Magnetic resonance neurography: current perspectives and literature review. *Eur Radiol* 2018; **28**: 698–707. doi: https://doi.org/10.1007/s00330-017-4976-8
75. Manoliu A, Ho M, Nanz D, Dappa E, Boss A, Grodzki DM, et al. Mr neurographic orthopantomogram: ultrashort echo-time imaging of mandibular bone and teeth complemented with high-resolution morphological and functional MR neurography. *J Magn Reson Imaging* 2016; **44**: 393–400. doi: https://doi.org/10.1002/jmri.25178
76. Zhu B, Liu JZ, Cauley SF, Rosen BR, Rosen MS. Image reconstruction by domain-transform manifold learning. *Nature* 2018; **555**: 487–92. doi: https://doi.org/10.1038/nature25988
77. Lundervold AS, Lundervold A. An overview of deep learning in medical imaging focusing on MRI. *Zeitschrift für Medizinische Physik* 2019; **29**: 102–27Available from. doi: https://doi.org/10.1016/j.zemedi.2018.11.002